Applied Surface Science Advances 32 (2026) 100929

Contents lists available at ScienceDirect

Applied Surface Science Advances

journal homepage: www.sciencedirect.com/journal/applied-surface-science-advances

Full Length Article

Role of Cu doping in promoting diffusion-assisted evolution of magnetic properties in equiatomic FeNi films

Ashish Gupta [a], Deepak Prajapat [b], Ilya Sergeev [b], Rajeev Joshi [a], Rajeev Rawat [a], Anil Gome [a], V.R. Reddy [a], Mukul Gupta [a,*]

[a] UGC-DAE Consortium for Scientific Research, University Campus, Khandwa Road, Indore 452001, India
[b] Deutsches Elektronen-Synchrotron DESY, Notkestrasse 85, 22607, Hamburg, Germany

ARTICLE INFO

Keywords:
Rare-earth-free permanent magnets
Chemically homogeneous FeNi multilayers
Nuclear resonance reflectivity
Self-diffusion
Mössbauer spectroscopy
Nuclear resonance scattering

ABSTRACT

The increasing need for environment-friendly substitutes for rare-earth-based magnets has sparked interest in materials such as the $L1_0$-ordered FeNi (tetrataenite) phase, which possesses high magnetocrystalline anisotropy and saturation magnetization. Despite being a promising candidate, preparation of this ordered phase in the laboratory remains a challenge due to the slow diffusion kinetics that prevent atomic ordering under normal conditions. From the theoretical estimations and experimental results, Cu is known for accelerating the atomic interdiffusion and promoting chemical disorder, which may facilitate the grain boundary diffusion. In the present work, chemically homogeneous multilayers of equiatomic FeNi and Cu-doped FeNi (5 at.%) were studied to investigate the correlation between self-diffusion and magnetism. Nuclear resonance reflectivity and forward scattering measurements on as-deposited and annealed samples showed that Cu doping substantially increases self-diffusion, which is in agreement with significant changes in the local magnetic environment, as supported by conversion electron Mössbauer spectroscopy. Although the net magnetic moment remained nearly unchanged, an enhancement in the coercivity at 573 K was observed in the Cu-doped sample, as quantified by SQUID-VSM. These observations highlight the potential of Cu-assisted diffusion channels to facilitate the formation of ordered phases in FeNi systems as a strategic approach to the development of rare-earth-free permanent magnets.

1. Introduction

In recent years, constraints in the availability of resources globally have created vulnerabilities in the critical element supply chain, and the cost of rare-earth elements has been rising. This intensified the search for high-performance rare-earth-free permanent magnets and research directed toward the materials composed of the less critical elements, often referred to as gap magnets [1–3]. Among them, the $L1_0$-ordered FeNi alloy (also known as tetrataenite) is remarkable due to its excellent set of properties, such as high saturation magnetization ($M_S \approx 1270$ emu/cc) [4], high uniaxial magnetocrystalline anisotropy (~1 MJ/m^3) [5,6], low magnetization damping (α) = 0.013 [7], and high Curie temperature (T_c) ≈ 800 K [8]. These characteristics, combined with the natural abundance and low cost of Fe and Ni, render $L1_0$ FeNi a suitable alternative to traditional Nd-Fe-B and Sm-Co magnets.

Yet, the laboratory synthesis of $L1_0$ FeNi in bulk or thin film form is hindered by the extremely low atomic diffusivities of constituent elements at moderate temperatures and the thermodynamically unstable nature of its formation under ambient conditions [9]. The ordering from the disordered face-centered cubic (fcc) state to the $L1_0$ ordered state is a diffusion-controlled transformation and is largely restricted by the slow atomic mobility of Fe and Ni, especially below the order-disorder transition temperature (~600 K) [10,11]. To bypass the kinetic barrier, several methods have been utilized, such as ion irradiation [12], nitrogen insertion [13], monolayer engineering [14], high-pressure torsion technique [15], and elemental doping [16]. Among these approaches, which require specialized processing and multi-step synthesis routes, elemental doping has been found to be a comparatively easier path. Particularly, Cu doping has been found to be favorable in enhancing atomic diffusion and inducing chemical disorder to ease the ordering process [17–19]. Computational studies using Miedema's model [20] and experimental evidence indicate that Cu substitution changes the enthalpy of formation and can induce strain in the lattice through the Bain path, conducive to the stabilization of the

* Corresponding author.
E-mail address: mgupta@csr.res.in (M. Gupta).

https://doi.org/10.1016/j.apsadv.2025.100929
Received 4 October 2025; Received in revised form 22 December 2025; Accepted 30 December 2025
Available online 12 January 2026

metastable tetragonal phase [21]. Due to the low volume diffusivities around ~600 K [9], self-diffusion measurements in FeNi alloys remain challenging. Even grain boundary diffusion is minimal (around 10^{-23} m^2/s at 573 K), necessitating highly sensitive characterization techniques [22]. The preparation of thin films and their analysis led to a deeper understanding of $L1_0$ ordered FeNi formation and its utilization in various fields. For instance, molecular beam epitaxy (MBE) and sputtering with co-deposition or multilayer deposition of Ni and Fe followed by rapid thermal annealing are widely explored [14]. Therefore, the current work focuses on equiatomic undoped and Cu-doped FeNi samples grown by multilayer deposition, and this approach aims to elucidate the role of Cu in facilitating the Fe self-diffusion and its connection to the development of magnetic ordering and local structure. In these multilayer thin films of alternating FeNiCu and isotopically labeled ^{57}FeNiCu layers, self-diffusion refers to the movement of atoms of the same element either within one layer or between interfaces. This diffusion occurs mainly via a vacancy-mediated mechanism, where atoms hop into neighboring vacant lattice sites [23]. To investigate self-diffusion in such systems, isotopic labeling is necessary since it provides contrast only between isotopes but ensures chemical homogeneity throughout the structure. These systems are thus referred to as chemically homogeneous multilayers (CHMs) [24]. In nanocrystalline multilayers, grain boundaries are fast diffusion pathways, as they facilitate atomic mobility due to their high density [25]. Interface roughness, lattice strain, and structural defects are some of the other factors that also contribute to the enhancement of the intermixing between layers [26]. Isotopic diffusion (e.g., of ^{57}Fe into the FeNiCu layer) can be successfully monitored by isotope-sensitive methods like nuclear resonance reflectometry (NRR) or Mössbauer spectroscopy, which offer the necessary sensitivity to resolve isotopic migration [27]. Nevertheless, the study of self-diffusion at the sub-nanometer level requires high-depth resolution. For instance, secondary ion mass spectrometry (SIMS) or radioactive tracer techniques offer direct depth profiling with a resolution of a few nanometers, making them unsuitable for CHMs at the sub-nm level. Alternatively, x-ray reflectivity or diffraction can provide sub-nm resolution but lacks the isotopic contrast required for direct observation of self-diffusion. Thus, nuclear methods remain the most promising for precisely investigating self-diffusion in such multilayer structures [22].

In this study, FeNi thin films were prepared by the co-sputtering method near equiatomic compositions. During growth, Cu was doped into FeNi at a concentration of approximately 5 at.%. The samples were fabricated in the form of isotope multilayers [FeNiCu (10 nm)/^{57}FeNiCu (3 nm)]$_{10}$, and NRR and nuclear resonant scattering (NRS) measurements were performed after annealing at various temperatures: 573, 673, 723, 748, and 773 K. Structural, diffusion, Mössbauer, local, and bulk magnetization measurements were conducted on these samples. It was observed that Cu doping significantly increases the self-diffusion of Fe and also affects the evolution of local magnetic environments. These findings support the idea of controlled atomic interdiffusion and highlight the role of Cu as a facilitator in the low-temperature stabilization of FeNi phases with favorable magnetic properties.

2. Sample preparation and experimental techniques

Multilayer samples of undoped and Cu-doped FeNi were prepared by depositing them on Si (100) and amorphous SiO_2 substrates using a DC-magnetron sputtering system (AJA International Inc., ATC Orion-8). Due to the residual stresses generated during the sputtering process, thin films may delaminate if these stresses exceed the material's cohesive or adhesive strength [28]. To mitigate this, the deposition was carried out at an elevated temperature of 473 K. The nominal multilayer structures as presented in Fig. 1(a) and (b) are [FeNi (10 nm)/^{57}FeNi (3 nm)]$_{10}$ for undoped samples and [FeNiCu (10 nm)/^{57}FeNiCu (3 nm)]$_{10}$ for Cu-doped samples, where FeNiCu indicates a 5 at.% Cu in FeNi. The deposition power of Fe and Ni targets was optimized to achieve an equiatomic FeNi ratio, while the ^{57}Fe target was prepared by placing ^{57}Fe foils in the racetrack of a natural Fe target [29]. A base pressure of 8 $\times$ 10^{-6} Pa was achieved before deposition. Both samples were deposited under an Ar flow of 50 sccm with a background pressure of 0.4 Pa, while all other deposition parameters were maintained as in our earlier study [19]. Post-deposition, the samples underwent isochronal annealing at temperatures (T_A) of 573, 673, 723, 748, 773, and 873 K for 1.5 hours under a vacuum of 1.33 $\times$ 10^{-3} Pa. Different annealing temperatures were chosen for each characterization technique based on its specific sensitivity for structural and diffusion-induced changes. Characterization techniques utilized include energy-dispersive x-ray spectroscopy (EDS), x-ray diffraction (XRD), X-ray reflectivity (XRR), NRR, and NRS. The EDS measurements were carried out using an Axia Chemi SEM (Thermo Fisher Scientific), with an accelerating voltage of 15 kV and a chamber pressure of approximately 10^{-2} Pa. XRD and XRR measurements were conducted with Cu K_α radiation (λ = 1.54 Å) using Bruker D8 Advance and D8 Discover systems. Conversion electron Mössbauer spectroscopy (CEMS) measurements were carried out using a PC-based spectrometer with a homemade gas flow counter. For room temperature measurement, a 96% He–4% CH_4 gas mixture was used, where He reduces the multiple scattering of conversion electrons, and CH_4 acts as a quenching gas. The spectra were recorded using a 50 mCi ^{57}Co (Rh) single-line source.

NRS was employed to assess the magnitude and orientation of magnetic hyperfine fields at both bulk and interface regions of FeNi multilayers. These measurements were performed at the nuclear resonance beamline P01 at PETRA III, DESY (Deutsches Elektronen-Synchrotron, Hamburg), using 14.4 keV x-rays corresponding to the ^{57}Fe Mössbauer transition. All samples were mounted in a fixed grazing incidence geometry, without any applied magnetic field [30]. The synchrotron operated in a 40-bunch mode with a 192 ns bunch separation. An avalanche photodiode detector with ~1 ns time resolution was used for NRS. Separation of nuclear (NRR) and electronic (XRR) signals was based on the delayed nature of nuclear transitions, given the 140 ns

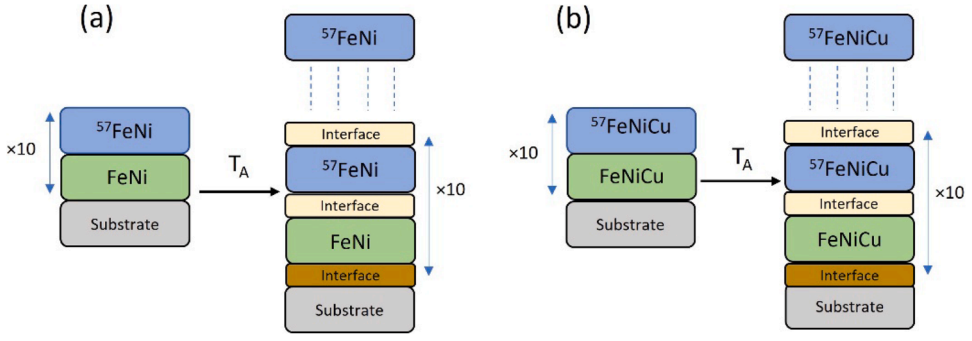

Fig. 1. Schematic diagram of undoped (a) and Cu-doped (b) FeNi chemically homogeneous multilayers for the pristine state and after annealing at T_A = 573, 673, 723, 748, 773, and 873 K.

lifetime of the Mössbauer excited state of ^{57}Fe. Electronic scattering (XRR) was detected within a few nanoseconds of the X-ray pulse, while NRR and NRS patterns were collected between 10-160 ns after the pulse. Bulk magnetic properties were investigated through magnetization measurements using a Quantum Design superconducting quantum interference device vibrating sample magnetometer (MPMS SQUID–VSM).

3. Results and discussion

3.1. Structural measurement

The chemical composition of the samples was confirmed by EDS with Fe (47.3 ± 0.2) % and Ni (52.7 ± 0.3) % in the undoped FeNi samples. In Cu-doped samples, its concentration was about 5 at.%.

Fig. 2 (a) and (b) show the XRD patterns of both undoped and Cu-doped FeNi multilayer samples. The undoped samples, including the pristine and annealed up to 873 K, exhibit a polycrystalline nature. The dominant diffraction peak observed at 2θ = 43.9° is attributed to the (111) plane of the face-centered cubic (fcc) FeNi structure (space group: $Fm\bar{3}m$) [31], accompanied by weaker reflections at 51.38° and 75.38°. The crystallite size (CS), estimated from the dominant (111) peak using the Scherrer equation [32], is approximately 20 nm for the pristine sample and increases to around 23 nm after annealing, indicating grain growth with thermal treatment. The typical error in the estimation of the CS is about 1 nm. Similarly, the Cu-doped FeNi samples also exhibit a polycrystalline fcc structure, with a major peak at 2θ = 43.9° and a minor peak at 51.4°. The CS of the doped sample is smaller, around 16 nm, and increases to approximately 21 nm after annealing at 873 K. The comparatively smaller CS in the Cu-doped films may be attributed to the structural disorder introduced by Cu incorporation. This interpretation aligns with the following observations from NRS and Mössbauer spectroscopy, which also suggest increased local disorder in Cu-containing samples, as discussed in later sections.

The XRR pattern of both samples, as shown in Figure S1(a) and (b) in the supplementary material, essentially yields a pattern analogous to a homogeneous thin film deposited on a Si substrate and therefore confirms the absence of any electronic contrast as expected in CHM. The thickness obtained from the fitting of the reflectivity curves using the GenX software [33] comes out to be 129 nm.

3.2. Diffusion measurements

Fig. 3(a) and (b) compare NRR patterns of undoped and Cu doped samples in the pristine state as well as after annealing at different temperatures within the q-range of 0.04 to 0.09 Å^{-1}, where q is the momentum transfer vector related to incident angle θ by $q = \frac{4\pi}{\lambda}\sin\theta$.

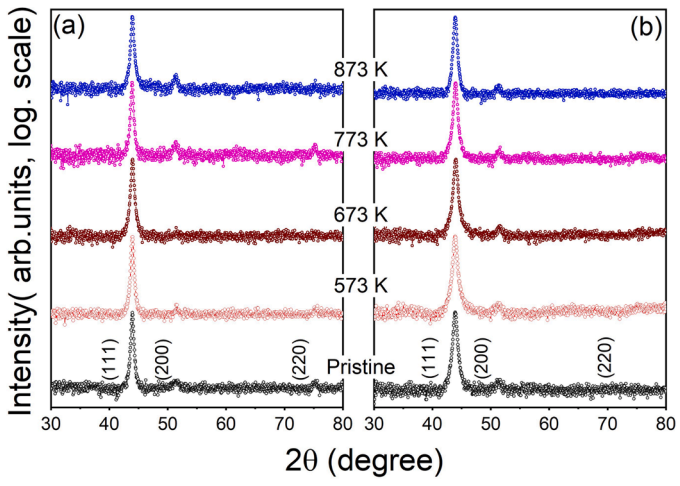

Fig. 2. XRD pattern of undoped (a) and Cu-doped (b) FeNi chemically homogeneous multilayers for pristine and annealed samples at T_A = 573, 673, 773, and 873 K.

The complete NRR patterns are provided in the supplementary material, Figure S2(a) and (b).

When the incident radiation energy is adjusted to match the nuclear resonance energy of ^{57}Fe (14.4 keV), a significant scattering contrast arises between the natural Fe and ^{57}Fe-enriched layers due to the strong nuclear resonance scattering from ^{57}Fe nuclei. Nuclear resonant scattering can be measured in two modes: (i) the time-integrated or angle-resolved mode, known as NRR, and (ii) the time-differential or time-resolved mode, known as NRS [34]. In the time-resolved (NRS) mode, the delayed nuclear decay photons are collected as a function of time within a fixed time window, whereas in the NRR mode, the delayed decayed photons are integrated over time and recorded as a function of the incident angle. At resonance energy, the total scattering amplitude (f) becomes [22]

$$f = f_e + f_n$$

where f_e and f_n are the electronic and nuclear scattering amplitudes, respectively. The refractive index (n) of the sample is given by [24,35]

$$n = 1 + \frac{\lambda_0^2}{2\pi}\sum_i \sigma_i (f_i^e + f_i^n)$$

where λ_0 is the wavelength of incident X-rays, and σ_i is the atomic density of the i^{th} species. Since f_n is significant only for ^{57}Fe, a strong scattering contrast emerges between natural Fe and ^{57}Fe-enriched layers, giving rise to a distinct Bragg peak (q_B) that appears around q = 0.07 Å^{-1} corresponding to the multilayer periodicity [36]. In NRR, the critical angle near $q_c \approx 0.05$ Å^{-1} appears as a peak resulting from interference between the incident and reflected waves, forming a standing wave with an antinode at the interface. When this antinode overlaps with the ^{57}FeNi layers, nuclear excitation is enhanced, giving rise to pronounced peaks in the NRR spectra [37,38]. Upon thermal annealing, the Bragg-peak intensity decreases due to Fe diffusion across the isotopic interfaces. This reduces the isotope contrast, causing a systematic decrease in the nuclear Bragg peak intensity. When the diffusion length becomes comparable to or greater than the layer thickness, the Bragg peak diminishes. Using the as-deposited peak intensity as a reference, the change in intensity is fitted using a Gaussian profile (after removing the q^{-4} Fresnel reflectivity dependence) to extract the diffusion coefficient D at each temperature, following the relation [39]:

$$\mathrm{I(T)} = \mathrm{I(0)}\exp\left(\frac{-8\mathrm{n}^2\pi^2\mathrm{D(T)}}{\mathrm{d}^2}\mathrm{t}\right) \quad (1)$$

The reflected intensities before and after annealing the multilayer (ML) at temperature T for a duration of t are represented as $I(0)$ and $I(T)$, respectively. The diffusion coefficient at temperature T is denoted as $D(T)$, while d represents the bilayer period, and n corresponds to the order of the Bragg reflection (with $n = 1$ in this study). Using Eq. 1, the diffusion coefficient D was determined by evaluating $I(T)$ and $I(0)$, which were extracted from the Bragg peak intensities. The bilayer period d and t is a known experimental parameter.

Based on the calculated values of D, the diffusion length L_d was estimated to be [40]:

$$L_d = \sqrt{2\mathrm{D(T)t}} \quad (2)$$

and the resulting values are summarized in Table 1.

In the undoped samples, a gradual reduction in the intensity of the first-order Bragg peak was observed with thermal annealing due to the diffusion of Fe across the isotopic interfaces. The value of the self-diffusion coefficient in the undoped sample at 573 K is 6.38 × 10^{-23} m^2/s, which increases to 4.24 × 10^{-22} m^2/s at 773 K.

In the context of the Cu-doped sample, the Bragg peak remains intact

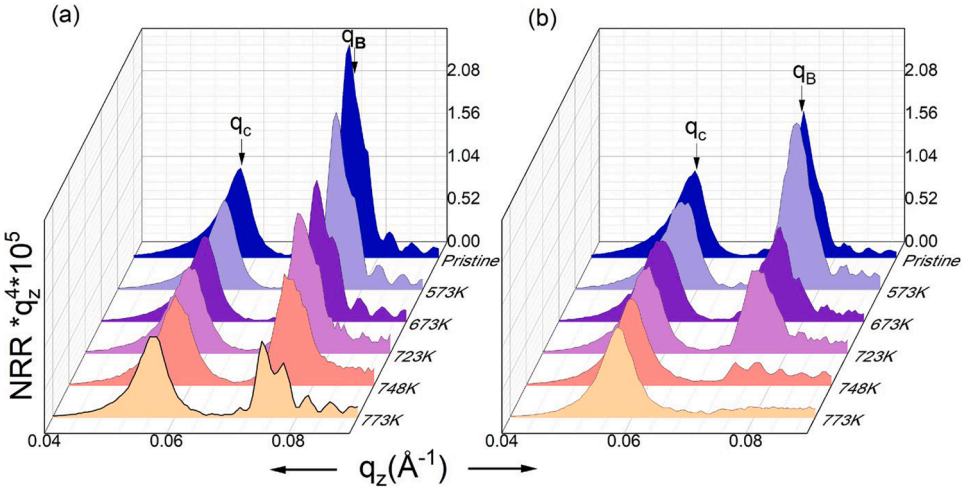

Fig. 3. Comparison of the intensity of the first-order Bragg peak of undoped (a) and Cu-doped (b) FeNi chemically homogeneous multilayers for pristine and annealed samples at T_A = 573, 673, 723, 748, and 773 K. The q_c and q_B represent the critical momentum transfer (corresponding to the critical angle) and Bragg momentum transfer (corresponding to multilayer periodicity), respectively.

Table 1
Diffusivity (D) and diffusion length (L_d) obtained from NRR measurements of undoped and Cu-doped multilayers at different annealing temperatures (T_A).

T_A (K)	FeNi		FeNiCu	
	D (m^2/s)	L_d (nm)	D (m^2/s)	L_d (nm)
573	6.38×10^{-23}	0.8	-	-
673	1.57×10^{-22}	1.3	2.01×10^{-22}	1.4
723	1.78×10^{-22}	1.3	2.27×10^{-22}	1.5
748	2.73×10^{-22}	1.7	8.98×10^{-22}	3.1
773	4.24×10^{-22}	2.1	Diffused	-

at 573 K without a notable change in intensity. After annealing at higher temperatures of 673 K and 723 K, the suppression of the Bragg peak infers an increased self-diffusion in Cu-doped samples, although not much increase is seen in the value of self-diffusion compared to the undoped sample. Further annealing at 748 K results in a four times increment in self-diffusion, and at 773 K, the multilayers are completely diffused. Therefore, a significant increment in the self-diffusion was observed after Cu doping in FeNi multi-layers. Further, the values of the diffusion coefficient obtained at different temperatures are used to calculate the activation energy E_a by using [41]:

$$D = D_0 exp\left(\frac{-E_a}{k_B T}\right) \quad (3)$$

where k_B is the Boltzmann constant, and T is the annealing temperature in Kelvin. Fig. 4(a) and (b) show the temperature dependence of diffusivity (ln D vs. 1000/T) for the undoped and Cu-doped FeNi samples, respectively. The Arrhenius behavior describes the temperature dependence of diffusion, reaction rates, and many physical processes in solids, and the activation energy is obtained from the slope of these plots.

The undoped FeNi sample (Fig. 4(a)) follows a linear Arrhenius trend; fitted data yield an Fe self-diffusion activation energy of 0.32 eV. The Cu-doped FeNi sample (Fig. 4(b)), however, shows deviation from simple Arrhenius behavior. Such deviations can arise when the dominant diffusion mechanism changes with temperature, possibly due to the activation of short-circuit diffusion paths associated with grain boundaries or internal interfaces. At low temperatures, these boundaries provide shorter pathways for atomic diffusion [24,42]. The high difference in the interfacial enthalpies of Cu with Fe and Ni and atomic size mismatch played a key role in short-to medium-range chemical segregation [21]. Additionally, Cu can alter vacancy formation and migration energies, leading to a distribution of diffusion barriers rather than a single activation energy [43]. This behavior can be studied by molecular dynamics simulations as well because this could validate with the experimental findings where Cu exhibits high atomic mobility and perturbs the surrounding Fe/Ni lattice, enhancing vacancy formation and promoting substitutional jumps without disrupting crystallinity [23].

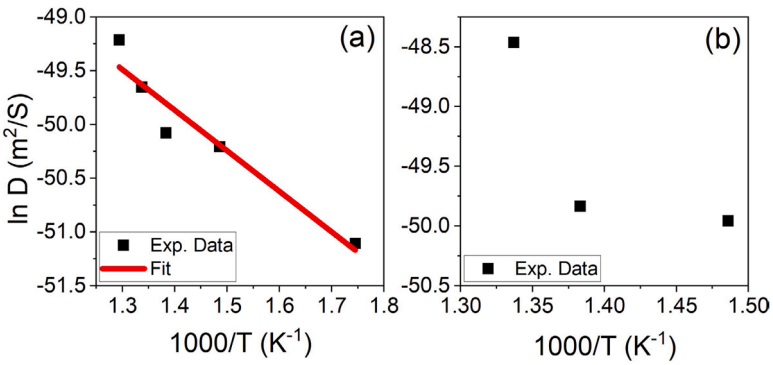

Fig. 4. Temperature dependence of diffusivity in undoped (a) and Cu-doped (b) FeNi chemically homogeneous multilayers. The straight-line fit in (a) is obtained using the relation $D = D_0 \exp(-E_a/k_B T)$.

3.3. Magnetization measurements

The magnetic hyperfine interactions from the ^{57}FeNi layers were investigated using CEMS combined with NRS techniques. Fig. 5(a) and (c) depict the CEMS spectra for the pristine and annealed (748 K) undoped FeNi samples, while Fig. 5(b) and (d) present the pristine and annealed (748 K) spectra for the Cu-doped FeNi samples. Each observed CEMS spectrum was fitted by using the NORMOS SITE and DIST fitting programs, where the SITE function (a, b, c, d) gives the relative area of different hyperfine components, and the DIST function (a′, b′, c′, d′) provides the probability distribution of distinct components [44]. The normalized χ^2 values for the spectra 5(a), (b), (c), and (d) are 1.23, 0.68, 1.04, and 1.08, respectively.

The obtained values are shown in Table 2. For both the as-deposited and annealed samples, the Mössbauer spectra exhibit a well-defined sextet, confirming that the films are magnetically ordered at room temperature, and as shown in the Fig. 5 (a′, b′, c′, d′), the hyperfine field spectral profile of all samples were characterized by a broad, intense peak centered around 30 T, typical of the disordered taenite (FeNi) phase. To extract more detailed information about the magnetic environments, all spectra were deconvoluted into three distinct sub-spectral components: 2 high-field components (S1 and S3) and a low-field component (S2). For the pristine undoped FeNi sample, hyperfine fields of approximately 32.2 T (S3), 29.9 T (S1), and 4.2 T (S2) were obtained, where S1 and S3 components occur from the probe Fe atoms located in different nearest neighbor configurations with varying Ni content in the first coordination shell, consistent with recent Mössbauer studies on FeNi alloys [15,45]. The low-field component S2 is attributed to a weak magnetic component, possibly arising from Fe atoms in defect-rich or low-coordination environments, such as grain boundaries or interfaces [46,47]. After annealing at 748 K, a few noticeable changes in hyperfine parameters and the relative intensity of the spectral components are observed in Fig. 5(c). The increased intensity of the main sextet indicates a higher volume fraction of the FeNi alloy phase, suggesting enhanced atomic ordering. The stability of the S1 and S3 component contributions and a slight reduction in the weak magnetic component further point towards the improved local magnetic ordering upon thermal treatment.

In the as-deposited Cu-doped FeNi sample, the spectrum exhibited a broad peak near 30 T, alongside a weak contribution around 4 T, which is depicted in Fig. 5(b). The spectral fitting yields three hyperfine field components: 31.09 T (S3), 28.58 T (S1), and 4.5 T (S2). The S3 and S1 components correspond to FeNi alloy phases with slightly different local environments or compositions [48]. The enhanced intensity of the S2 component, compared to the undoped sample, suggests that Cu doping introduces additional weak magnetic sites. This might be the result of the increased local disorder, strain, or the disruption occurring in the magnetic coupling among Fe atoms due to Cu atoms [49]. Following annealing at 748 K, as illustrated in Fig. 5(d), there is a slight increase in the hyperfine field values, consistent with enhanced magnetic exchange interactions due to improved alloying and reduced structural disorder. More significantly, the relative area of the low-field component decreases sharply, becoming nearly negligible (~1%). This declination indicates that annealing promotes the formation of a more magnetically homogeneous phase, alleviating the disorder introduced by Cu doping.

Overall, the Mössbauer data confirm that both undoped and Cu-doped FeNi multilayers retain their magnetic ordering post-deposition and improve further upon thermal treatment. The observed shifts in hyperfine field distributions, particularly the increase in average magnetic field strength and reduction in the contribution of weak magnetic components, provide strong evidence of enhanced alloying and diffusion-assisted short-range magnetic homogenization after annealing. Furthermore, the influence of Cu doping is clearly reflected in the initial increase of weak magnetic component signal intensity, likely due to lattice strain and compositional fluctuations, which are effectively suppressed after annealing. These results promote the controlled atomic

Table 2
Mössbauer hyperfine parameters of FeNi and FeNiCu multilayer samples.

Sample	Site	H (T)	I.S. (mm/s)	Q.S. (mm/s)	Relative Area (%)
FeNi (pristine)	Sextet 1	29.92 ± 0.12	0.03 ± 0.005	0.05 ± 0.015	47.97 ± 6 4.62 ± 0.5
	Sextet 2	4.28 ± 0.28	0.22 ± 0.037	0.44 ± 0.037	47.41 ± 6
	Sextet 3	32.23 ± 0.13	0.05 ± 0.007	0.06 ± 0.007	
FeNi (Annealed 748 K)	Sextet 1	30.17 ± 0.07	0.032 ± 0.004	0.04 ± 0.008	50.11 ± 4 1.89 ± .5
	Sextet 2	2.26 ± 0.5	0.33 ± 0.062	0.21 ± 0.09	48.01 ± 3
	Sextet 3	32.45 ± 0.08	0.04 ± 0.005	0.05 ± 0.009	
FeNiCu (Pristine)	Sextet 1	28.58 ± 0.20	0.023 ± 0.01	0.062 ± 0.035	29.81 ± 7 11.63 ± 2
	Sextet 2	4.51 ± 0.71	0.24 ± 0.09	0.30 ± 0.209	58.56 ± 8
	Sextet 3	31.09 ± 0.15	0.034 ± 0.15	0.028 ± 0.023	
FeNiCu (Annealed 748 K)	Sextet 1	29.89 ± 0.03	0.04 ± 0.002	0.04 ± 0.004	60.35 ± 1 1.09 ± .1
	Sextet 2	4.68 ± 0.04	0.03 ± 0.12	0.12 ± 0.097	38.56 ± 2
	Sextet 3	32.37 ± 0.02	0.04 ± 0.003	0.08 ± 0.003	

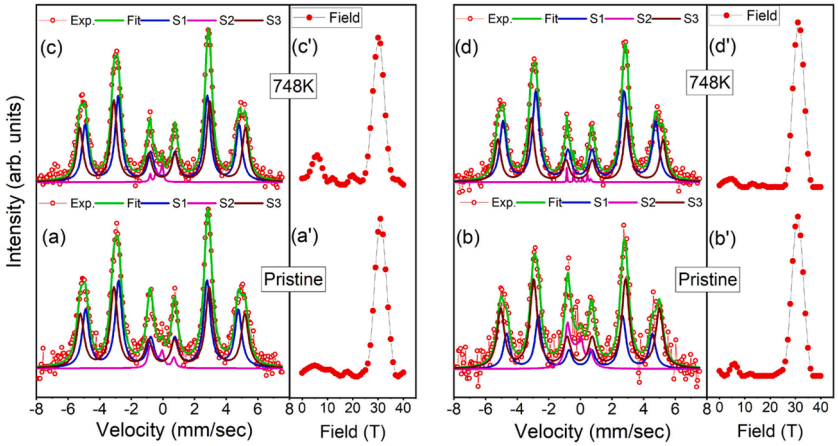

Fig. 5. CEMS spectra and corresponding fits using the SITE (a, c) and DIST (a′, c′) functions for undoped FeNi multilayers, and SITE (b, d) and DIST (b′, d′) functions for Cu-doped FeNi multilayers, shown in the pristine state (a, b) and after annealing at T_A = 748 K (c, d).

diffusion as well as support the role of Cu as a catalyst for accelerating the atomic mobility and promoting the short-range intermixing at moderate annealing temperatures.

Fig. 6(a) and (b) illustrate NRS spectra of undoped and Cu-doped samples following isochronal annealing at different temperatures, measured at the q_c. The NRS pattern is utilized in modeling magnetic and spin alignment in the ^{57}FeNi layers. The time-domain oscillations in the NRS spectra arise from the splitting of the nuclear hyperfine levels of ^{57}Fe due to the interaction of the nuclear quadrupole moment with the surrounding electronic charges [50]. The spectra were analyzed using the REFTIM software package, which simulates time-resolved nuclear forward scattering based on dynamical theory [51]. The NRS fitting was initiated with roughly estimated hyperfine field values obtained from the fitting of CEMS data, and the final values were obtained through iterative refinement until the simulated time spectra reproduced the experimental oscillations. The fitting yields quantitative information about the magnitude and the orientation of the local magnetic moment [52]. The main fitting parameters include the hyperfine magnetic field (B_{hf}), its distribution width (ΔB_{hf}), and the orientation of the magnetic hyperfine field. The field orientation is defined by two angles: β, the angle with respect to the surface normal, and γ, the azimuthal angle with respect to the direction of x-ray polarization [37,53]. ΔB_{hf} represents the distribution of hyperfine fields around the mean value B_{hf}. Additionally, the NRS fitting yields other hyperfine parameters, such as the isomer shift (IS) and the electric field gradient (EFG). The isomer shift quantifies changes in the electron density at the Fe nucleus due to variations in local bonding or composition, whereas the EFG describes the magnitude of the electric field asymmetry of the charge distribution around the Fe nuclei [50].

Both pristine, undoped, and Cu-doped samples show well-defined quantum beats up to 65 ns, indicating magnetic ordering at room temperature. The quantum beat pattern exhibits signs of disorder at 573 K and 673 K; however, it becomes progressively sharper from 723 K onward, indicating better magnetic ordering and the development of a more uniform hyperfine field. This trend is also supported by the fitting results, which show narrower ΔB_{hf} distributions at elevated temperatures. The fitting of these spectra yielded three hyperfine components: a major fraction around ~30 T corresponding to the disordered FeNi (taenite) phase, a minor high-field component near ~32 T attributed to Fe-rich regions, and a low-field component around ~4.5 T associated with weakly magnetic environments also observed in the CEMS measurements. In Cu-doped samples, the beat pattern is slightly more damped, possibly due to increased disorder or a higher fraction of weak magnetic component. These samples show a similar beat pattern but with more evident changes at lower temperatures. The dominant hyperfine field remains centered near 30 T, consistent with the disordered FeNi matrix, while the persistent ~4.5 T component in early annealed samples suggests that Cu doping initially promotes weak magnetic environments due to the static local disorder introduced by Cu atoms. With further annealing at higher temperatures (748 K and 773 K), the beat amplitude becomes sharper, suggesting that Cu doping may assist in faster atomic rearrangement and enhance FeNi ordering. From 723 to 773 K, both undoped and Cu-doped samples exhibit more coherent quantum beats and less contribution of the weak magnetic component, as seen by the reduced intensity of the ~4.5 T component. Notably, in the sample annealed at 573 K, the spectrum shows a slight splitting in the beat pattern. Since the detailed shape of the beat pattern depends on both the magnitude and the direction of the internal hyperfine field relative to the x-ray propagation vector [54], this indicates a change in the direction of the internal field, suggesting the emergence of locally distinct magnetic environments due to heterogeneous Cu distribution. The broader ΔB_{hf} values observed in the Cu-doped sample suggest that Cu incorporation leads to increased local magnetic field fluctuations, likely arising from structural disorder induced by diffusion or from variations in the local atomic environment (such as Fe–Fe, Fe–Ni, or Fe–Cu configurations). In undoped samples, the isomer shift (IS) values vary between ~ 0.08–0.34 mm/s, with slightly increasing trends upon annealing. These minor shifts hint at subtle electronic structure changes. In contrast, the Cu-doped samples exhibit a greater variation in IS values, reflecting more significant changes in the electronic surroundings [55]. Both systems show very low EFG values. However, in the Cu-doped samples, some of the less prominent Fe environments—referred to as minor components—exhibit slightly higher EFG, suggesting local asymmetries likely caused by the addition of Cu atoms. Angular distribution parameters (β, γ) confirm predominantly in-plane magnetic moments in the undoped sample, whereas the Cu-doped system shows slight angular reorientations, suggesting higher incoherent magnetic fractions or phase-separated domains, consistent with SQUID-VSM results. This trend supports thermally activated atomic diffusion and ordering. Thus, the hyperfine fields obtained from both CEMS and NRS match well, giving a clear and consistent view of the magnetic changes and structural transformation in both undoped and Cu-doped FeNi thin films during annealing.

Fig. 7 shows the room temperature M –H loops of undoped (a, c) and Cu-doped (b, d) chemically homogeneous multilayer FeNi samples, measured by applying the magnetic field in parallel (in-plane) and

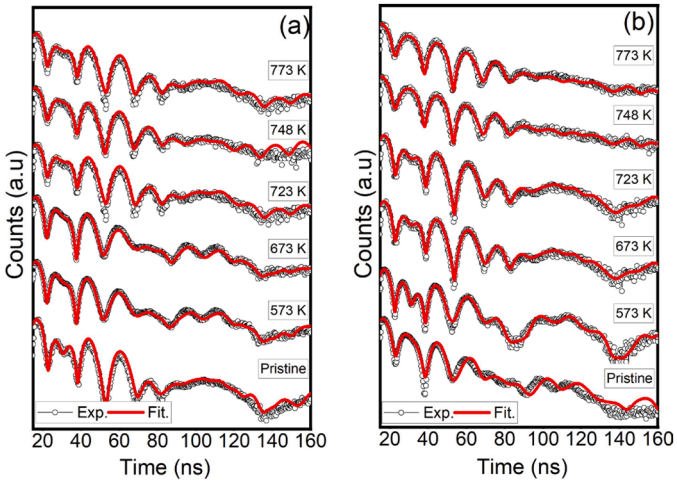

Fig. 6. NRS time spectra of undoped (a) and Cu-doped (b) FeNi chemically homogeneous multilayers as a function of annealing temperature T_A = 573, 673, 723, 748, and 773K. The best fit to experimental data is represented by a continuous curve.

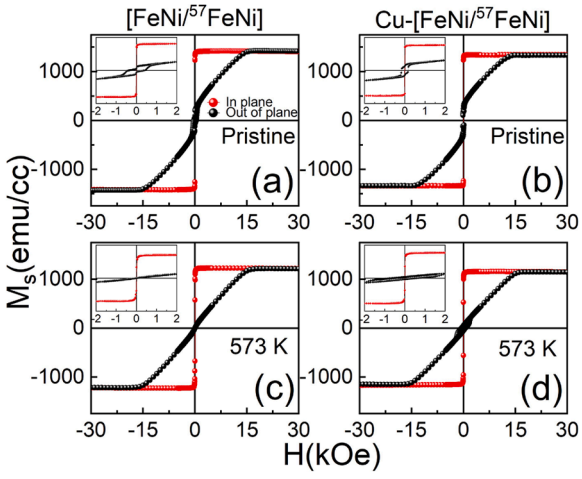

Fig. 7. Room temperature magnetization curves for undoped and Cu-doped FeNi samples in the pristine state (a, b) and after annealing at T_A = 573 K (c, d). In-plane and out-of-plane curves are represented by solid red and solid black circles, respectively. The inset panels represent the enlarged hysteresis curves.

perpendicular (out-of-plane) to the sample surface. M –H loops of all the samples exhibited clear ferromagnetic hysteresis at room temperature, consistent with the sextet structures observed in Mössbauer spectra and the magnetic time oscillations from NRS. The values of saturation magnetization (M_s) and out-of-plane coercivity ($H_c^{\perp}$) for all samples (pristine and annealed at 573 K) are summarised in Table 3. The in-plane coercivity is very small and falls within the experimental error; therefore, only the out-of-plane coercivity was reported.

The pristine, undoped FeNi samples demonstrated strong in-plane anisotropy with sharp hysteresis loops, which further improved upon annealing. This behavior is in agreement with the increased hyperfine fields and magnetic volume fractions observed at 748 K in CEMS. In the Cu-doped FeNi series, the magnetic loops initially showed a relatively soft hysteresis loop followed by increased coercivity after annealing at 573 K in the perpendicular direction. This coercivity enhancement was likely arising from enhanced domain-wall pinning due to diffusion-induced microstructural modifications, such as defect redistribution, compositional fluctuations, and possibly due to a small fraction of $L1_0$-ordered FeNi phase promoted by Cu incorporation [56–58]. This change aligns with the observed bifurcation in the NRS beating pattern at 573 K in the Cu-doped sample, which shows changes in the local magnetic environment. Also, the value of saturation magnetization (M_s) did not change significantly after Cu doping [59]. Furthermore, the M_s in both samples remained relatively unchanged after annealing at elevated temperatures. This behavior is also observed in various experimental studies on Fe-Ni alloys, where it is reported that Ms strongly depends on the temperature at low Ni concentrations, while at higher Ni concentrations ($x \sim 0.50$), M_s is temperature independent [60,61]. The out-of-plane hysteresis loops for both undoped and Cu-doped FeNi samples, in the pristine and annealed states, exhibit increased shearing, reduced symmetry, and incomplete saturation at applied low fields, which are consistent with previous studies in FeNi. This indicates the distribution of anisotropic axes because different regions of the film have slightly different preferred magnetization directions, and the magnetization reversal occurs over a range of fields consistent with the spatially varying local environments inferred from NRS and CEMS [14, 62–64].

Table 3
Magnetic parameters extracted from M-H hysteresis loops.

Sample name	Ms (emu/cc)	$H_c^{\perp}$ (Oe)
FeNi – Pristine	1340	370
FeNi – 573 K	1260	-
FeNiCu -Pristine	1310	160
FeNiCu -573 K	1170	570

4. Conclusion

In this work, the effect of Cu doping on the structural, self-diffusion, local, and bulk magnetization of the chemically homogeneous FeNi multilayers has been studied comprehensively. The undoped and Cu-doped FeNi multilayers were deposited in the same deposition conditions and were simultaneously annealed at different temperatures. The self-diffusion measurements performed using NRR suggested that Cu doping significantly enhanced the self-diffusion process, which augmented the local magnetic properties measured by NRS. The reduction in the weak magnetic component observed from the CEMS measurement validated improved crystallinity and local atomic ordering with annealing. The appearance of enhanced coercivity at 573 K may arise due to an $L1_0$ hard phase, which may be present along with the soft fcc FeNi phase. The insights gained from this study provide a deeper understanding of diffusion-assisted short-range ordering in FeNi-based systems, but do not provide the direct structural evidence for long-range $L1_0$ ordering. Therefore, future studies will explore time-dependent annealing strategies, annealing under an applied magnetic field, and advanced structural characterization using TEM/EDS and resonant X-ray diffraction. These investigations are beneficial for guiding the development of rare-earth-free magnetic materials with optimized performance.

CRediT authorship contribution statement

Ashish Gupta: Writing – review & editing, Writing – original draft, Visualization, Validation, Software, Methodology, Investigation, Data curation. **Deepak Prajapat:** Writing – review & editing, Visualization, Validation, Software, Resources, Data curation. **Ilya Sergeev:** Writing – review & editing, Visualization, Validation, Resources, Methodology. **Rajeev Joshi:** Writing – review & editing, Resources, Methodology, Investigation. **Rajeev Rawat:** Writing – review & editing, Visualization, Validation, Supervision, Resources. **Anil Gome:** Software, Methodology. **V.R. Reddy:** Writing – review & editing, Visualization, Supervision, Methodology, Investigation. **Mukul Gupta:** Writing – review & editing, Visualization, Validation, Supervision, Project administration, Methodology, Investigation, Funding acquisition, Conceptualization.

Declaration of competing interest

The authors declare that they have no known competing financial interests or personal relationships that could have appeared to influence the work reported in this paper.

Ashish Gupta reports financial support was provided by DST Inspire. Mukul Gupta reports equipment, drugs, or supplies and travel were provided by India-DESY Collaboration. If there are other authors, they declare that they have no known competing financial interests or personal relationships that could have appeared to influence the work reported in this paper.

Acknowledgements

Layanta Behera, Shailesh Kalal, Amit, Akshaya, and Nikita are acknowledged for their support in sample preparation, discussion, and XRD measurements. Sharanjeet Singh and Dileep Gupta are acknowledged for EDS measurements. A.G. Khanderao is acknowledged for NRS data analysis. A. J. Pal and V. G. Sathe are acknowledged for support. The authors gratefully acknowledge the Department of Science and Technology (DST), Government of India, for providing the funding through the India-DESY collaboration to carry out some part of this research work at the light source PETRA-III of DESY. AG also acknowledges DST Inspire for financial support.

Supplementary materials

Supplementary material associated with this article can be found, in the online version, at doi:10.1016/j.apsadv.2025.100929.

Data availability

Data will be made available on request.

References

[1] O. Gutfleisch, M.A. Willard, E. Brück, C.H. Chen, S. Sankar, J.P. Liu, Magnetic materials and devices for the 21st century: stronger, lighter, and more energy efficient, Adv. Mater. 23 (7) (2011) 821–842.
[2] S. Mandal, M. Debata, P. Sengupta, S. Basu, L10 FeNi: a promising material for next generation permanent magnets, Crit. Rev. Solid State Mater. Sci. 48 (6) (2023) 703–725.
[3] J. Cui, M. Kramer, L. Zhou, F. Liu, A. Gabay, G. Hadjipanayis, B. Balasubramanian, D. Sellmyer, Current progress and future challenges in rare-earth-free permanent magnets, Acta Mater. 158 (2018) 118–137.
[4] J. Paulevé, A. Chamberod, K. Krebs, A. Bourret, Magnetization curves of Fe–Ni (50–50) single crystals ordered by neutron irradiation with an applied magnetic field, J. Appl. Phys. 39 (2) (1968) 989–990.

[5] T. Kojima, M. Mizuguchi, T. Koganezawa, M. Ogiwara, M. Kotsugi, T. Ohtsuki, T. Tashiro, K. Takanashi, Addition of Co to L10-ordered FeNi films: influences on magnetic properties and ordered structures, J. Phys. D: Appl. Phys. 47 (42) (2014) 425001.

[6] J. Marciniak, M. Werwiński, Magnetic anisotropy of L10 FeNi (001),(010), and (111) ultrathin films: a first-principles study, J. Magn. Magn. Mater. 609 (2024) 172455.

[7] M. Ogiwara, S. Iihama, T. Seki, T. Kojima, S. Mizukami, M. Mizuguchi, K. Takanashi, Magnetization damping of an L1-FeNi thin film with perpendicular magnetic anisotropy, Appl. Phys. Lett. 103 (24) (2013).

[8] P. Wasilewski, Magnetic characterization of the new magnetic mineral tetrataenite and its contrast with isochemical taenite, Phys. Earth Planet. Inter. 52 (1-2) (1988) 150–158.

[9] N. Bordeaux, A.M. Montes-Arango, J. Liu, K. Barmak, L.H. Lewis, Thermodynamic and kinetic parameters of the chemical order–disorder transformation in L10 FeNi (tetrataenite), Acta Mater. 103 (2016) 608–615.

[10] E. Dos Santos, J. Gattacceca, P. Rochette, G. Fillion, R. Scorzelli, Kinetics of tetrataenite disordering, J. Magn. Magn. Mater. 375 (2015) 234–241.

[11] L.-Y. Tian, H. Levämäki, O. Eriksson, K. Kokko, Á. Nagy, E.K. Délczeg-Czirják, L. Vitos, Density functional theory description of the order-disorder transformation in Fe-Ni, Sci. Rep. 9 (1) (2019) 8172.

[12] L. Amaral, R. Scorzelli, M. Brückman, A. Paesano, J.E. Schmidt, T. Shinjo, N. Hosoito, Very thin Fe/Ni modulation multilayer films under ion bombardment, J. appl. phys. 81 (8) (1997) 4773–4775.

[13] K. Ito, T. Ichimura, M. Hayashida, T. Nishio, S. Goto, H. Kura, R. Sasaki, M. Tsujikawa, M. Shirai, T. Koganezawa, et al., Fabrica- tion of L10-ordered FeNi films by denitriding FeNiN (001) and FeNiN (110) films, J. Alloys Compd. 946 (2023) 169450.

[14] K. Takanashi, M. Mizuguchi, T. Kojima, T. Tashiro, Fabrication and characterization of L10-ordered FeNi thin films, J. Phys. D: Appl. Phys. 50 (48) (2017) 483002.

[15] M. Kołodziej, J.-M. Greneche, S. Auguste, J. Marcin, J. Kovac, B. Idzikowski, Z. Śniadecki, Triggering chemical segregation in the meteorite-based FeNi alloys by severe plastic deformation and magnetic-field-assisted annealing, J. Alloys Compd. (2025) 182545.

[16] L.-Y. Tian, O. Gutfleisch, O. Eriksson, L. Vitos, Alloying effect on the order–disorder transformation in tetragonal FeNi, Sci. Rep. 11 (1) (2021) 5253.

[17] Y.K. Takahashi, M. Ohnuma, K. Hono, Effect of cu on the structure and magnetic properties of FePt sputtered film, J. Magn. Magn. Mater. 246 (1–2) (2002) 259–265.

[18] K. Sharma, G. Sharma, M. Gupta, V.R. Reddy, A. Gupta, Enhancement of L1 transformation in Fe/Pt multilayer by cu addition, AIP Adv. 8 (10) (2018).

[19] A. Gupta, S. Kalal, A. Akshaya, J. Stahn, M. Gupta, Study of interdiffusion and Magnetization of Cu-doped Fe/Ni multilayers, J. Supercond. Nov. Magn 37 (8) (2024) 1661–1667.

[20] H. Bakker, Enthalpies in alloys, Mater. Sci. Found. 1 (1998) 1–78.

[21] M. Kołodziej, Z. Śniadecki, The formation of structural disorder in FeNi-based alloys–Theoretical approach, Mater. Lett. 326 (2022) 132917.

[22] M. Gupta, Synthesis, stability and self-diffusion in iron nitride thin films: A review, Recent Adv. Thin Films (2020) 131–179.

[23] G. Dai, S. Wu, X. Huang, M. Wang, X. Teng, Thermal diffusion behavior of Fe/Cu/Ni multilayer coatings: a molecular dynamics study, Model. Simul. Mater. Sci. Eng. 30 (6) (2022) 065003.

[24] A. Gupta, M. Gupta, S. Chakravarty, R. Rüffer, H.-C. Wille, O. Leupold, Fe diffusion in amorphous and nanocrystalline alloys studied using nuclear resonance reflectivity, Phys. Rev. B—Condens. Matter Mater. Phys. 72 (1) (2005) 014207.

[25] A. Tiwari, M.K. Tiwari, M. Gupta, H.-C. Wille, A. Gupta, Interface sharpening in miscible and isotopic multilayers: Role of short-circuit diffusion, Phys. Rev. B 99 (20) (2019) 205413.

[26] A. Paul, Effect of interface roughness on magnetic multilayers of Fe/Tb and Fe/Cr, J. Magn. Magn. Mater. 240 (1–3) (2002) 497–500.

[27] A. Tayal, M. Gupta, N. P. Lalla, A. Gupta, M. Horisberger, J. Stahn, K. Schlage, H. C. Wille, Effect of dopants on thermal stability and self-diffusion in iron-nitride thin films, Phys. Rev. B 90 (14) (2014) 144412.

[28] G. Abadias, E. Chason, J. Keckes, M. Sebastiani, G.B. Thompson, E. Barthel, G. L. Doll, C.E. Murray, C.H. Stoessel, L. Martinu, Stress in thin films and coatings: Current status, challenges, and prospects, J. Vac. Sci. Technol. A 36 (2) (2018).

[29] P. Kumar, V. Reddy, V. Ganesan, M. Gupta, I. Sergueev, O. Leupold, H.C. Wille, Structural and magnetic properties of co-sputtered $Fe_{0.8}C_{0.2}$ thin films, Phys. Rev. Mater. 4 (1) (2020) 013402.

[30] H. Wille, H. Franz, R. Röhlsberger, W. Caliebe, F. Dill, Nuclear resonant scattering at PETRA III: Brilliant opportunities for nano–and extreme condition science, J. Phys.: Conf. Ser. 217 (2010) 012008. IOP Publishing.

[31] A. Lutts, P. Gielen, The order-disorder transformation in $FeNi_3$, Phys. Status Solidi 41 (1) (1970) K81–K84.

[32] F.T.L. Muniz, M.R. Miranda, C. Morilla dos Santos, J.M. Sasaki, The Scherrer equation and the dynamical theory of X-ray diffraction, Found. Crystallogr. 72 (3) (2016) 385–390.

[33] A. Glavic, M. Björck, Genx 3: the latest generation of an established tool, Appl. Crystallogr. 55 (4) (2022) 1063–1071.

[34] A.G. Khanderao, I. Sergueev, H. Wille, D. Kumar, Interface resolved magnetism at metal–organic (Fe/Alq3) interfaces under x-ray standing wave condition, Appl. Phys. Lett. 116 (10) (2020).

[35] K. Schlage, R. Röhlsberger, Nuclear resonant scattering of synchrotron radiation: Applications in magnetism of layered structures, J. Electron Spectrosc. Relat. Phenom. 189 (2013) 187–195.

[36] A. Gupta, X-ray and neutron studies of nanoscale atomic diffusion in thin films and multilayers, Appl. Surf. Sci. 256 (2) (2009) 552–557.

[37] R. Röhlsberger, J. Bansmann, V. Senz, K. Jonas, A. Bettac, K. Meiwes- Broer, O. Leupold, Nanoscale magnetism probed by nuclear resonant scattering of synchrotron radiation, Phys. Rev. B 67 (24) (2003) 245412.

[38] L. Deák, L. Bottyán, D.L. Nagy, Calculation of nuclear resonant scattering spectra of magnetic multilayers, Hyperfine Interact. 92 (1994) 1083–1088.

[39] H. Schmidt, M. Gupta, T. Gutberlet, J. Stahn, M. Bruns, How to measure atomic diffusion processes in the sub-nanometer range, Acta mater. 56 (3) (2008) 464–470.

[40] S. Amir, M. Gupta, A. Gupta, Surfactant controlled interfacial alloying in thermally evaporated Cu/Co multilayers, J. Alloys Compd. 522 (2012) 9–13.

[41] M. Gupta, A. Gupta, J. Stahn, T. Gutberlet, Ordering and self-diffusion in FePt alloy film, New J. Phys. 10 (5) (2008) 053031.

[42] H. Mehrer, Point defects in crystals, Diffusion in solids: Fundamentals, methods, materials, Diff.-Control. Pro. (2007) 69–93.

[43] H. Mehrer, Diffusion in intermetallics, Materials Transactions, JIM 37 (6) (1996) 1259–1280.

[44] R.A. Brand, Normos Mössbauer fitting program, user's guide, Wissenschaftlich Elektronik GmbH, Starnberg, 1995.

[45] L.H. Lewis, P.S. Stamenov, Accelerating nature: induced atomic order in equiatomic FeNi, Adv. Sci. 11 (7) (2024) 2302696.

[46] M. Pires, M. Araujo Filho, J. Tedesco, J. Ardisson, W. Macedo, Out-of-plane magnetic anisotropy in columnar grown Fe–Ni films, J. Phys. Chem. Solids 75 (10) (2014) 1124–1131.

[47] F. Genuzio, T. Menteş, K. Freindl, N. Spiridis, J. Korecki, A. Locatelli, Chemistry-dependent magnetic properties at the FeNi oxide–metal interface, J. Mater. Chem. C 8 (17) (2020) 5777–5785.

[48] T. Huang, Z. Song, A. Jain, Y. Wang, Role of Cu in tailoring the structure and soft magnetic performance of Fe-based nanocrystalline alloys during two-step annealing, J. Mater. Sci.: Mater. Electron. 36 (10) (2025) 1–12.

[49] P. Panissod, J. Durand, J. Budnick, Hyperfine fields in metallic glasses, Nucl. Instrum. Methods Phys. Res. 199 (1-2) (1982) 99–114.

[50] G. Sharma, A. Gupta, M. Gupta, K. Schlage, H.C. Wille, In situ small-angle x-ray and nuclear resonant scattering study of the evolution of structural and magnetic properties of an Fe thin film on MgO (001), Phys. Rev. B 92 (22) (2015) 224403.

[51] M. Andreeva, Nuclear resonant reflectivity data evaluation with the "REFTIM" program, Hyperfine Interact. 185 (2008) 17–21.

[52] R. Röhlsberger, Coherent elastic nuclear resonant scattering. Nuclear condensed matter physics with synchrotron radiation: basic principles, methodology and applications, Springer, 2005, pp. 67–180.

[53] R. Röhlsberger, H. Thomas, K. Schlage, E. Burkel, O. Leupold, R. Rüffer, Imaging the magnetic spin structure of exchange-coupled thin films, Phys. Rev. lett. 89 (23) (2002) 237201.

[54] M. Andreeva, B. Lindgren, Nuclear resonant spectroscopy at bragg reflections from periodic multilayers: basic effects and applications, Phys. Rev. B—Condens. Matter Mater. Phys. 72 (12) (2005) 125422.

[55] A. Kozioł-Rachwał, T. Giela, B. Matlak, K. Matlak, M. Ślęzak, T. Ślęzak, M. Zając, R. Rüffer, J. Korecki, Magnetism of ultrathin fe films in MgO/Fe/MgO in epitaxial structures probed by nuclear resonant scattering of synchrotron radiation, J. Appl. Phys. 113 (21) (2013).

[56] P. Sharma, Y. Zhang, A. Makino, Magnetic properties of L10 FeNi phase developed through annealing of an amorphous alloy, IEEE Trans. Magn. 53 (11) (2017) 1–10.

[57] K. Dev, R. Kaur, G. Vashisht, I. Sulania, S. Annapoorni, Magnetization reversal behavior in electrodeposited Fe–Co–Ni thin films, IEEE Trans. Magn. 58 (8) (2022) 1–7.

[58] M. Ghafari, H. Hahn, T. Feng, R. Kruk, M. Yan, On the relationship between magnetic moment and nuclear magnetic hyperfine field of ^{57}Fe, Hyperfine Interact. 242 (1) (2021) 2.

[59] Z. Rao, B. Dutta, F. Körmann, D. Ponge, L. Li, J. He, L. Stephenson, L. Schäfer, K. Skokov, O. Gutfleisch, et al., Unveiling the mechanism of abnormal magnetic behavior of FeNiCoMnCu high-entropy alloys through a joint experimental-theoretical study, Phys. Rev. Mater. 4 (1) (2020) 014402.

[60] A. Sahoo, A.A. Biswal, S. Parida, V. Medicherla, S.S. Behera, M. Singh, A. Sagdeo, S. Datta, A. Singh, K. Maiti, Electronic, magnetic and thermal behavior near the invar compositions of Fe-Ni alloys, J. Electron Spectrosc. Relat. Phenom. (2025) 147540.

[61] N.S. Kanhe, A. Kumar, S. Yusuf, A. Nawale, S. Gaikwad, S.A. Raut, S. Bhoraskar, S. Y. Wu, A. Das, V. Mathe, Investigation of structural and magnetic properties of thermal plasma-synthesized $Fe_{1-x}Ni_x$ alloy nanoparticles, J. Alloys Compd. 663 (2016) 30–40.

[62] Y. Wang, P. Sharma, A. Makino, Magnetization reversal in a preferred oriented (111) L10 FePt grown on a soft magnetic metallic glass for tilted magnetic recording, J. Phys.: Condens. Matter 24 (7) (2012) 076004.

[63] R. Raj, M. Kuila, M. Gupta, V.R. Reddy, ^{57}Fe mössbauer and magneto-optical Kerr effect (MOKE) study of transcritical state in permalloy (Fe_xNi_{100-x}) thin films, Hyperfine Interact. 242 (2021) 19.

[64] A. Svalov, I. Aseguinolaza, A. Garcia-Arribas, I. Orue, J. Barandiaran, J. Alonso, M. Fernández-Gubieda, G. Kurlyandskaya, Structure and magnetic properties of thin permalloy films near the "transcritical" state, IEEE Trans. Magn. 46 (2) (2010) 33333.